High current operation of a storage-ring free-electron laser

R. Roux, M. E. Couprie,* R. J. Bakker,† D. Garzella,* D. Nutarelli,* L. Nahon,* and M. Billardon‡
Laboratoire pour l'Utilisation du Rayonnement Electromagnetique, Bâtiment 209D, Université Paris–Sud, 91405 Orsay Cedex, France
(Received 26 January 1998; revised manuscript received 23 July 1998)

The operation of storage-ring free-electron lasers (SRFEL) at high current still represents a challenge because of the growth of longitudinal beam instabilities. One of these, the quadrupolar coherent synchrotron oscillation, is very harmful for free-electron-laser (FEL) operation. On the Super-ACO storage ring, they either prevent the FEL start-up, or result in a very poor stability of the FEL source. A new feedback system to damp the quadrupolar coherent synchrotron oscillation has been installed on the ring and the stabilized beam parameters have been systematically measured. As a result, the FEL gain is higher and the FEL operates more easily and with a higher average power. Its stability, which is very critical for user applications, has been significantly improved as it has been observed via systematic measurements of FEL dynamics performed with a double sweep streak camera. [S1063-651X(98)10011-9]

PACS number(s): 41.60.Cr, 41.60.Ap

I. INTRODUCTION

Free-electron lasers are coherent tunable sources that presently cover the wavelength range from IR to the UV. Their principle lies on the interaction between an electromagnetic wave stored in an optical cavity and a relativistic electron beam traveling through the magnetic field of an undulator [1]. Because of the requirement of a higher electron beam energy with good quality for the ultraviolet radiation, FELs have been developed either on linear accelerators (FELI [2], Los Alamos [3]) or on storage rings, following the first successful operation of a SRFEL on Anneau de Collisions d'Orsay (ACO), Orsay collision ring [4].

The length of the SRFEL optical resonator must be carefully chosen to satisfy the longitudinal synchronization requirement between electron bunches and light pulses (i.e., the ''detuning condition''): The electron revolution time in the ring must be a multiple of the photon round-trip time in the cavity. Moreover, the tuning of the laser is precisely adjusted by changing the electron revolution period through a slight modification of the storage ring rf cavity frequency. The laser temporal structure is intimately related to the detuning between electron bunches and laser pulses stored in the optical cavity. The laser can be either quasi ''continuous,'' i.e., reproducing the periodicity of the bunches, or pulsed (due to some beam instabilities or detuning operation). The maximum average power and the minimum temporal width of the laser micropulse are obtained at the perfect tuning.

The gain of the FEL depends both on the beam parameters (energy, electron density) and on the insertion device characteristics. The temporal features of the Super-ACO FEL are described in Table I. We find that operating at the nominal energy of the ring is more compatible with normal users of synchrotron radiation, providing reasonable lifetime and power for applications. The Super-ACO FEL is ''cw'' at perfect tuning but the laser micropulse can present an important jitter resulting either from residual longitudinal instabilities of the beam and/or from a slow drift, which probably derives from thermal expansion of the cavity mirrors.

First applications using the Super-ACO FEL were performed in 1993 in biology [5] on a coenzyme molecule. One advantage of a SRFEL is the natural synchronization between the laser and synchrotron radiation light pulses. This has allowed the combination of both sources, for the performance of a pump-probe experiment to study the surface photovoltage effect in semiconductors [6]. These experiments motivated a study of the laser temporal behavior [7,8] in order to improve the stability of the laser and to increase its average power. First, a longitudinal feedback [9] efficiently reduces the jitter of the laser micropulse (also fast drifts of the laser, probably due to sudden beam position jumps). The drift of the laser position, measured by the dissector [10,11], is compensated by a change of the rf frequency so that the laser is brought back into perfect synchronism. The FEL can be kept stable over 10 h with very few readjustments of mirrors.

Nevertheless, above 60 mA in the ring, parasitic electric fields can arise due to the complex interaction between the electron bunches and the vacuum chamber and induce strong perturbations of the electrons. Depending on their frequency and their location, these fields can lead to a motion of the whole bunch, called coherent synchrotron oscillations [12]

TABLE I. List of the Super-ACO FEL temporal structure parameters at perfect tuning.

Repetition rate	8.32 MHz
Temporal width	50 ps
Spectral width	0.6 Å
Maximum jitter	200 ps
Resonance frequency	300 Hz

*Present address: CEA/SPAM, Centre d'etude de Saclay, 91191 Gif-sur-Yvette, France.
†Present address: Bessy II, Geb. 15.1, Rudower Chaussee 5, D-12489 Berlin, Germany.
‡Present address: ESPCI, 10 rue Vauquelin, 75231 Paris Cedex, France.

TABLE II. Beam parameters of the Super-ACO storage ring: E_S, nominal energy of the ring, T_S, revolution time of the electrons in the ring, V_{rf} and f_{rf}, rf cavity voltage and frequency, respectively, α, momentum compaction factor, $U(E_S)$, energy lost by synchrotron radiation per turn, f_s, synchrotron frequency, τ_s, synchrotron damping time, σ_γ/γ, value of the energy spread at quasizero current and σ_e, bunch length (rms) at quasizero current, σ_X and σ_Z bunch transverse sizes (rms) in the undulator, L_{und} the length of one undulator of the FEL optical klystron.

E_S (MeV)	800
T_S (ns)	240
V_{rf} (kV)	170
f_{rf} (MHz)	100
α	0,0142
$U(E_S)$ (keV)	21
f_s (kHz)	14
τ_s (ms)	10
$\frac{\sigma_\gamma}{\gamma}$ at 0 mA	$5{,}4.10^{-4}$
σ_e at 0 mA (ps)	86
σ_X and σ_Z (μm)	380 and 390
L_{und} (m)	1,3

and dramatically reduce the laser gain [13]. The gain is proportional to the electronic density and therefore the laser has the largest growth rate at the maximum of the electron bunch density. If the bunch average position is longitudinally oscillating at, for example, the coherent synchrotron frequencies of the nth order, the laser cannot follow the bunch position as the laser time constants are very long (see Tables I and II). In this case the laser keeps a constant position while the bunch oscillates around it, so that the laser gain oscillates as a function of $e-(a\ \sin n\Omega_s t)^2/2\sigma_e^2$, a being the amplitude of the coherent synchrotron oscillations, $\Omega_s/2\pi$ its frequency, and σ_e the rms bunch length. Averaging over the period of the oscillation leads to a gain reduction proportional to $e^{-a^2/4\sigma_e^2}$. In addition the laser is sensitive to a low frequency evolution of the amplitude of the coherent synchrotron oscillations and laser instabilities appear in the frequency range of $\approx$0–500 Hz. Such behavior is generally seen whatever the frequency and the type of oscillations (dipolar, quadrupolar, etc.) might be and is only governed by the amplitude of the oscillation. The laser stability is extremely sensitive to gain variations; oscillations of a few picoseconds are sufficient to degrade it, thus these must be reduced to improve the laser stability.

This paper analyzes natural behavior of the electron beam, its stabilization, and consequences for the FEL operation. The influence of the FEL on the beam is finally discussed.

II. NATURAL LONGITUDINAL BEHAVIOR OF THE ELECTRON BEAM AT HIGH CURRENT

In a storage ring, the transverse motion of the electrons is defined by the magnetic elements. In addition an rf cavity supplies the electrons with the energy lost by synchrotron radiation. Depending on the phase of the electrons with respect to the rf wave, they will be either accelerated or decelerated, leading to a bunching of the electrons around the synchronous particle for which the energy loss per turn is exactly compensated by the rf cavity.

A. Longitudinal single particle motion and bunch lengthening

Because of the energy loss by emission of synchrotron radiation and the compensation due to the rf field, the electrons naturally undergo damped sinusoidal oscillations at the synchrotron frequency f_s, with the synchrotron damping time τ_s (see Table II). The motion of each electron in the bunch is not coherent with the others because the interactions (collisions between electrons, different positions on the rf voltage slope, quantum emission of synchrotron radiation, etc.) are different for each particle. Thus the stationary solution of the Fokker-Planck equation leads to a Gaussian distribution of energy and position of the electrons in the bunch. At quasizero current, the bunch length σ_e, the rms width of the electronic temporal distribution, is proportional to the energy spread σ_γ/γ according to

$$\sigma_e=\frac{\alpha}{\Omega_s}\frac{\sigma_\gamma}{\gamma}, \tag{1}$$

with $\Omega_s=2\pi f_s$ and α being the momentum compaction factor.

However, for higher currents, bunch instabilities appear and induce a blowup of the bunch length called ''anomalous bunch lengthening'' [14]. This effect, widely observed in storage rings, is attributed to the complex interaction between the beam and the ring vacuum chamber or resonators. The frequency spectrum of the bunch can spread over several GHz for the usual rf frequency of a few hundred MHz (100 MHz in the Super-ACO case). Parasitic high-frequency electric fields are induced by the impedance of the ring pipe (kickers and vacuum vessels). These parasitic fields lead to the so-called potential-well distortion resulting in incoherent bunch lengthening. In addition, these fields may induce the so-called microwave instability leading to both an increase of the energy spread and an incoherent bunch lengthening. On new storage rings [15,16], vacuum chambers are designed to be as smooth as possible, with fewer cross-section jumps and with special features to minimize the impedance.

B. Coherent synchrotron oscillations

Above a given threshold of current, coherent instabilities arise in which all electrons in the bunch can oscillate coherently at the synchrotron frequency and its harmonics either in position and/or in profile shape. These oscillations can be measured with a spectrum analyzer (Fig. 1) connected to a beam pick-up electrode. At low current, dipolar modes of coherent synchrotron oscillation may appear and the bunch centroid moves sinusoidally at the synchrotron frequency f_s. These dipolar modes are damped by a Pedersen-type feedback [17]. Between 60 and 110 mA, the quadrupolar modes at $\approx 2f_s$ are established and overlap with sextupolar modes at $\approx 3f_s$ around 90 mA. Figure 2 shows double sweep streak camera (DSSC) images [18,19,20], clearly illustrating the evolution of the bunch distribution shape versus time. In the

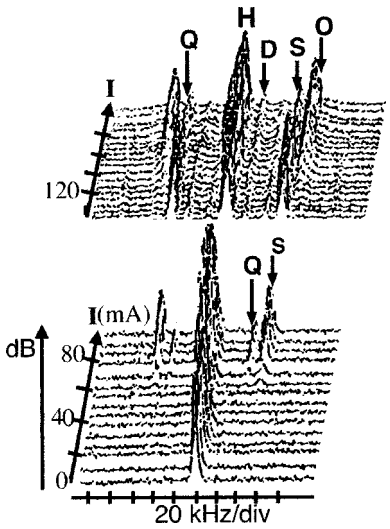

FIG. 1. Evolution of sidebands as a function of the total current I (20 mA/div), measured with a Marconi spectrum analyzer centered on the 292nd harmonic (H) of the revolution frequency. The vertical scale is the amplitude in dB. Dipolar modes (D) are damped by a feedback, coherent synchrotron oscillations of a growing order appear vs the current: quadrupolar modes (Q) at 26.6 kHz, sextupolar modes (S) at 37 kHz, and octupolar modes (O) at 46.4 kHz.

quadrupolar mode [Fig. 2(a)], the bunch distribution symmetrically shortens and lengthens with respect to the center, while in a sextupolar mode [Fig. 2(b)], the distribution deforms asymmetrically. In the 120–200-mA range, octupolar modes at $\approx 4 f_s$ are present.

The sextupolar and quadrupolar modes have also been measured in the time domain with the dissector and the DSSC; the results are shown in the Figs. 3 and 4, respectively. In Figs. 3(a) and 3(c), the intensity is modulated at 2 and 3 times the synchrotron frequency. Figure 3(b) shows an intermediate case where both types of synchrotron oscillations are present. However, the measurement with the dissector only gives the frequency of the coherent synchrotron oscillations and does not allow one to clearly distinguish between a position variation and shape deformation of the bunch distribution. In fact, as displayed in Fig. 4, the rms value of the bunch length oscillates with the frequency of the quadrupolar coherent synchrotron oscillation mode, inducing a periodic variation of the intensity at any point in the electronic distribution. Note that the amplitude of the quadrupolar motion is rather important, 60 ps peak-peak, representing 30% of the average bunch length.

III. STABILIZATION OF THE ELECTRON BEAM WITH A FEEDBACK ON THE QUADRUPOLAR MODES

A feedback system to damp the quadrupolar coherent synchrotron oscillations was developed and installed on Super-ACO in February 1996 (Fig. 5). Quadrupolar oscillations are detected with a pick-up electrode on the 288th harmonic of the bunch revolution frequency. Passing through a mixer at 1.2 GHz to get rid of the 288th harmonic and a pass-band filter centered on 28 kHz ($\approx 2 f_s$), the signal is used to modulate the rf cavity voltage after loop phase and gain adjustments to cancel the quadrupolar oscillations.

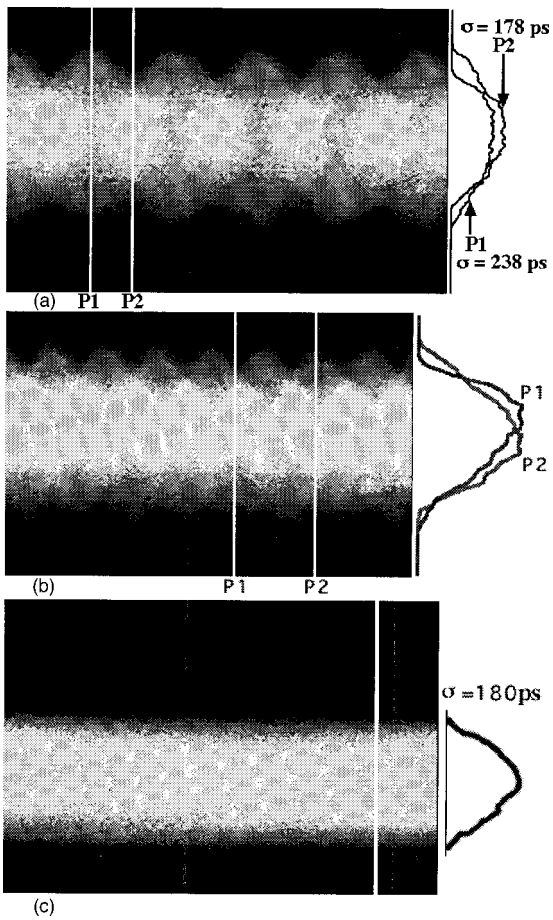

FIG. 2. Double sweep streak camera images. Horizontal range=200 μs, vertical range=1.7 ns. (a) $I=94$ mA, quadrupolar coherent synchrotron oscillation; (b) sextupolar modes, $I=110$ mA. Examples of electronic density profiles ($P1$ and $P2$) are displayed on the right-hand side of the figure. In (c) $I=80$ mA with the quadrupolar feedback damping the quadrupolar coherent synchrotron oscillation, the bunch shape is no longer deformed as in (a). A profile of the electronic density corresponding to a vertical slice of the image is displayed on the right.

The operation of this feedback system modifies the longitudinal behavior. All beam characteristics, relevant from the FEL point of view, have been measured with the quadrupolar feedback in operation and compared with the case without feedback.

A. Coherent synchrotron oscillations

The quadrupolar feedback (QFB) system appears to be quite effective and reliable. Figure 6 shows measurements made with the spectrum analyzer for three current values. The quadrupolar feedback clearly damps quadrupolar oscillations with respect to the usual situation without feedback over the whole current range where they are present. In addition, the current threshold of the sextupolar coherent synchrotron oscillations is lowered to 84–85 mA, in contrast with 90 mA previously. Probably, in this current range, the competition between the quadrupolar and the sextupolar modes has disappeared thereby allowing the sextupolar coherent synchrotron oscillations to start and develop more

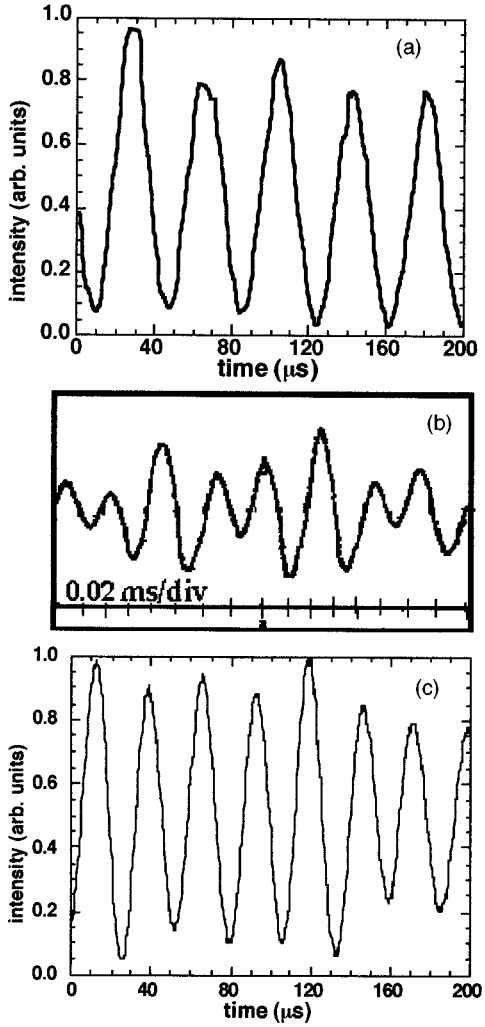

FIG. 3. Measurements of coherent synchrotron oscillations using the dissector in the phase oscillation mode: plain quadrupolar mode in (a), mixed quadrupolar and sextupolar modes in (b), and plain sextupolar mode in (c).

easily. Temporal measurements with the DSSC [Fig. 2(c)] show that the bunch distribution shape is not deformed as in Fig. 2(a) and remains stable below the sextupolar synchrotron oscillations threshold.

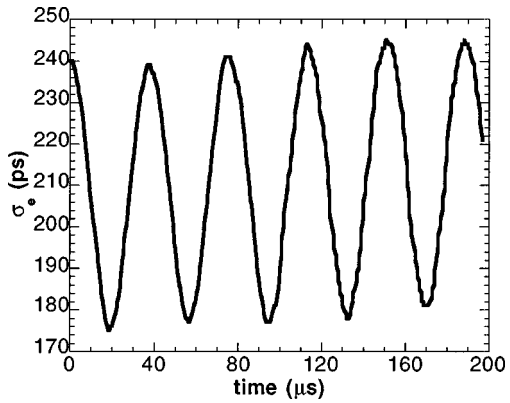

FIG. 4. Quadrupolar mode of coherent synchrotron oscillation for $I=94$ mA with two stored bunches, the rms bunch length σ_e vs time [data from Fig. 2(a)].

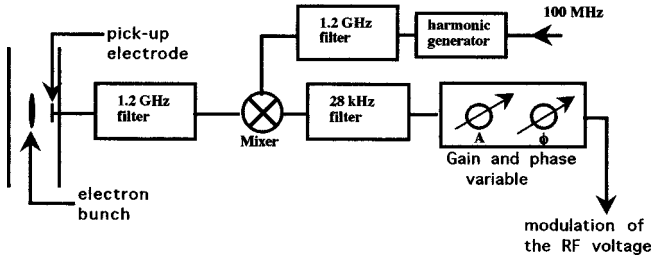

FIG. 5. Sketch of the feedback damping the quadrupolar coherent synchrotron oscillations.

B. Bunch length versus current

In the presence of the QFB, the bunch length could be modified. As this parameter is a critical one for the FEL operation, measurements have been performed with two diagnostic systems, dissector and DSSC. As the bunch shapes generally deviate from a Gaussian distribution, the data have been treated using the moment method, based on the statistic calculation of the mean value and the root mean square of the distribution without any assumption of shape.

The analysis of measurements shows that the evaluation of the rms bunch length assuming a Gaussian distribution is 30% larger (on average) than that obtained with the moment method. In fact, the agreement with the theory predicting a Gaussian electronic distribution is only verified at very low current before the beginning of the potential well distortion regime.

Figures 7(a) and 7(b) show the measurements of bunch length made using the dissector and the DSSC, respectively with QFB and without QFB as a function of the total current in the ring. The agreement between the two kinds of measurements is rather good. However, there is a slight discrepancy that grows with current. This could be due to the very

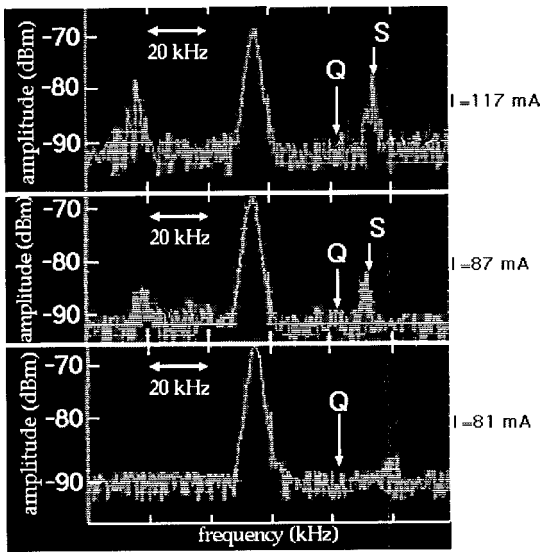

FIG. 6. Images of the Marconi spectrum analyzer, the vertical axis stands for the amplitude in dB m and the horizontal axis the frequency (20 kHz/div). In order to have a clear detection of sidebands, the measurements are made close to the 292nd harmonic of the revolution frequency. The amplitude of the sextupolar mode (S) of coherent synchrotron oscillation decreases and no quadrupolar modes (Q) appear because of the quadrupolar feedback.

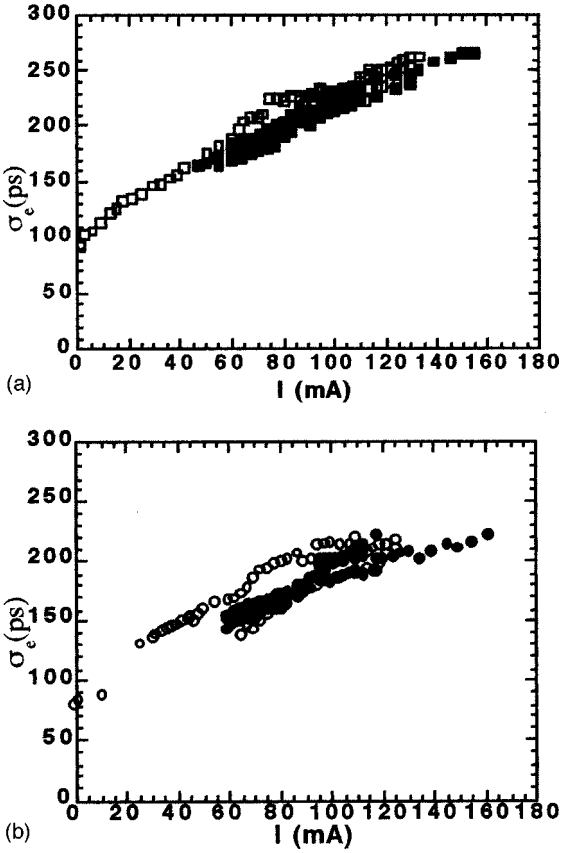

FIG. 7. RMS bunch length σ_e vs the total current, in the two bunch mode measured using the dissector, (a): QFB on (■), QFB off (□); using the DSSC, (b): QFB on (●), QFB off (○). The dissector takes 3.3 ms to measure the longitudinal distribution while the double sweep streak camera, only a few μs. The intensity of the light pulses measured by the DSSC are only sampled over 8 bits, namely, 256 levels.

different acquisition times for the two detectors. At high current, the bunch is shaken by the phase oscillations, which can fluctuate in amplitude during the dissector acquisition period. Besides, it appears that the average bunch length in the presence of the quadrupolar coherent synchrotron oscillations is not very different from its value when the oscillations are suppressed with the QFB.

C. Energy spread versus current

The evolution of the energy spread versus beam current is an important issue not only for FEL operation but also for the knowledge of the various instability regimes of the longitudinal beam behavior. The Super-ACO FEL uses an optical klystron to enhance the laser gain. This insertion device is composed of two permanent magnet undulators separated by a dispersive section that produces a strong magnetic field to reinforce the microbunching effect. Usually, the energy spread is deduced from the measurement of the beam horizontal dimension in a ring dispersive section. However, we prefer to use a more sensitive method based on the measurement of the synchrotron radiation emitted by the optical klystron [21]. The emission spectrum of the latter is a set of fringes resulting from the interference between the emission in each undulator. One defines a fringe modulation rate f, which depends on the energy spread σ_γ/γ as follows:

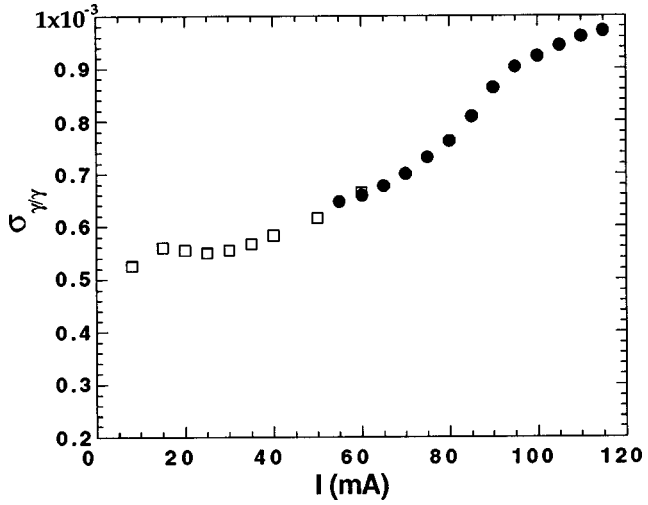

FIG. 8. Energy spread $\sigma_{\gamma/\gamma}$ vs the total current I, quadrupolar feedback off (□), and quadrupolar feedback on (●) measured using the optical klystron fringe method.

$$f = f_0 \exp -2\left(2\pi(N+N_d)\,\frac{\sigma_\gamma}{\gamma}\right)^2. \tag{2}$$

f_0 represents the contribution of the size, divergence, and position of the beam in the optical klystron and is constant (0.95) as a function of the current. $N+N_d$ is the interference order, depending on the gap of the dispersive section. The curve of σ_γ/γ versus current (Fig. 8) is deduced from the measurements of spectra for several gaps of the dispersive section as a function of the total current in the two bunches mode.

It is not possible to compare the energy spread, with and without quadrupolar feedback at high current because of the quadrupolar coherent synchrotron oscillation itself. The spectrum is deformed and the fringes are excessively blurred for precise measurements. However, the energy spread has been previously measured up to 60 mA (without the quadrupolar feedback) and we have been able to extend these measurements up to 115 mA (with a good overlap between both), even in the presence of sextupolar coherent synchrotron oscillations, with the quadrupolar feedback.

Between zero and 32 mA, the energy spread remains constant in the regime of potential-well distortion. Above 32 mA, in the microwave instabilities regime, the energy spread increases quickly versus current, growing very fast between 80 and 95 mA. This could be attributed to the rise of the sextupolar coherent synchrotron oscillations, which usually overlap with the quadrupolar modes of coherent synchrotron oscillations. The consequences could be quite dramatic for the operation of the FEL because the gain is proportional to the modulation rate.

The interaction of the electron beam with the vacuum chamber in a storage ring results in complex longitudinal behavior. Studies on the dynamics of the free-electron laser should rely on models taking into account anomalous bunch lengthening and the various types of instabilities. Experimental analysis on this subject is carried out in the following section.

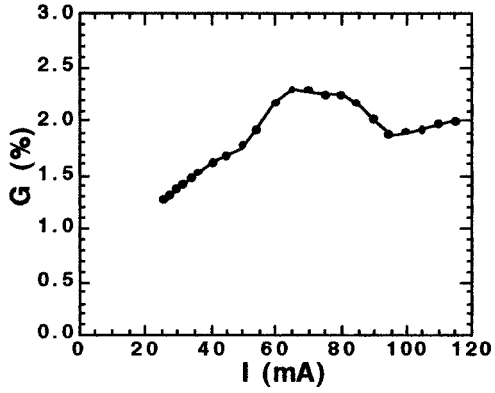

FIG. 9. Gain G of the Super-ACO FEL vs the total current I in the ring, with the QFB.

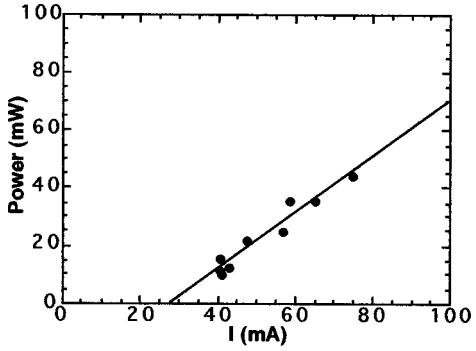

FIG. 10. Measurements of the average laser power transmitted through the two mirrors (●) and a linear fit (solid line).

IV. FEL PERFORMANCES

FEL characteristics such as average power, tunability, and emission spectral range in the UV are mainly determined by the laser gain, which strongly depends on the beam parameters (beam transverse sizes, bunch length, and energy spread) and losses of the optical cavity. Moreover, the stability and the availability of the shortest optical pulse widths are also critical issues for reliable application experiments using the FEL, thus most of our studies are dedicated to the accurate observation of the FEL temporal behavior.

A. FEL gain

The gain G, according to the theorem of Madey, is derived from the shape of the spontaneous emission spectrum of the optical klystron [22]. An optical klystron small signal gain can be expressed as [23]

$$G = 2.22\times 10^{-13} K^2 L_{ond}^2 (JJ)^2 (N+N_d) f \frac{\rho_e F_f}{\gamma^3}, \qquad (3)$$

with K the deflection parameter equal to $eB_0\lambda_0/2\pi mc$, λ_0 the magnetic field period, e and m represent the charge and the mass of the electron, respectively, c the light speed, B_0 the maximum vertical magnetic field on axis, L_{ond} the length of one undulator, $(JJ)=[J_0(\xi)-J_1(\xi)]$ the difference of Bessel functions with argument $\xi=K^2/(4+2K^2)$, ρ_e the electronic density, F_f the filling factor (taking into account the transverse overlap between the electron and photon beams), and γ the Lorentz factor.

G is evaluated versus the total current I in the ring (see Fig. 9) according to the bunch dimensions (Fig. 7) and energy spread measurements (Fig. 8) shown previously in the case of operation with the quadrupolar feedback.

At low current, the gain grows almost linearly with current, reaches its maximum between 65 and 70 mA, and decreases at higher current, i.e., the growth of the energy spread and the bunch length becomes larger than the linear increase of the current. The laser is usually operated below 80 mA, close to the maximum gain of the laser, because in this regime the sextupolar coherent synchrotron oscillations have disappeared. The stability is therefore improved and mirror heating and degradation due to the synchrotron radiation [24] are moderate. Though, in the case of user experiments requiring higher laser extracted power, the FEL has been operated at up to 120 mA.

B. Laser extracted power

According to the Renieri [30] limit, the average laser extracted power is proportional to the average power emitted by synchrotron radiation (synchrotron power) in a bending magnet of the storage ring. The synchrotron power is also proportional to the total current stored in the ring, and therefore the laser power should grow linearly with the current. Indeed, measurements (Fig. 10) of the total laser power useful for experiments (extracted from both sides of the optical cavity) confirm this relationship. Without the quadrupolar feedback, the laser could only be operated for users below the threshold of the quadrupolar coherent synchrotron oscillations, around 60 mA and the laser power was only 35 mW; now, with the quadrupolar feedback and the present mirrors set with a transmission of 0.01% one can operate the laser at 100 mA with a power of 70 mW with rather good stability. Taking into account the absorption of the cavity mirrors and the reflection of the sapphire interfaces, the total laser power extracted from the beam is 7.1 W at 100 mA. In the near future, we expect to increase the transmission (and therefore the useful laser power) by a factor 10 due to the recent installation of a new 500 MHz rf cavity, which enhances the laser gain by more than a factor 2.

C. Temporal structure

The laser width (rms value, evaluated from the moments of the micropulse distribution) depends strongly on the FEL stability. Indeed, at perfect tuning, after the saturation state has been reached by damped relaxation oscillations, the laser line should continue to narrow [25], but this requires a stable beam lasting from several 100 ms or 1 s. Measurements performed with the double sweep streak camera as a function of current show a very large dispersion (Fig. 11), because this condition is not always satisfied. One can observe a smaller width between 50 and 70 mA due to the lack of phase oscillations and one can reach rather low values even at very high current (12 ps at 94 mA) because of the longitudinal feedback, which allows the laser line narrowing to occur due to the reduction of the laser jitter. The average values of the width are shown in Table III. At lower current, the laser

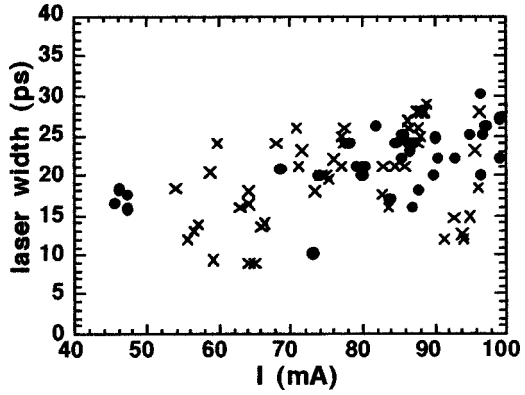

FIG. 11. QFB on, rms laser width vs the total current in the ring. Crosses are for measurements with the longitudinal feedback on, while circles are with feedback off.

temporal width is naturally smaller because the electronic density, from which it is generated, decreases as a function of the current.

D. Detuning curve

The maximum gain of the laser is obtained for perfect synchronism between the electron bunch and laser light pulse stored in the optical cavity. But, even for a slight detuning, the laser average power can adopt quite different temporal behaviors as a function of the detuning according to the so-called detuning curve. On the first SRFELs such as ACO, VEPP3, TERAS, and UVSOR, the laser intensity was pulsed at perfect synchronism and when detuned, became quasi cw as seen in the case of UVSOR with an optical klystron (see Fig. 2 in [19]). On Super-ACO, we usually distinguish five areas (see [26], Fig. 1) as illustrated in Fig. 12(d): at perfect synchronism, the laser is most powerful, quasi cw and has the smallest temporal and spectral width. However, it also suffers from a jitter and intensity fluctuations. For a small detuning, there are two zones where the laser is pulsed at 300 Hz, is less powerful and has larger widths (temporal and spectral) than in the previous case. For an even larger detuning, the laser becomes cw again with even less power and the largest widths. Recently, the UVSOR FEL obtained a cw regime at the perfect synchronism due to a new helical undulator and higher gain [27]. The detuning curve shape is actually determined by the laser gain, the bunch length, and the beam stability; therefore slightly different situations are observed for different SRFELs. The detuning curve has already been theoretically explained using a pass-to-pass longitudinal evolution model [28], taking into account the longitudinal detuning at low current (below 60 mA). So it appears that the laser intensity is an oscillator-type system in which damping time depends

TABLE III. FEL rms temporal width σ_L for three total current ranges.

Current range (mA)	σ_L (ps)
50–70	16±4.9
70–80	21±4.8
80–100	22.4±6.8

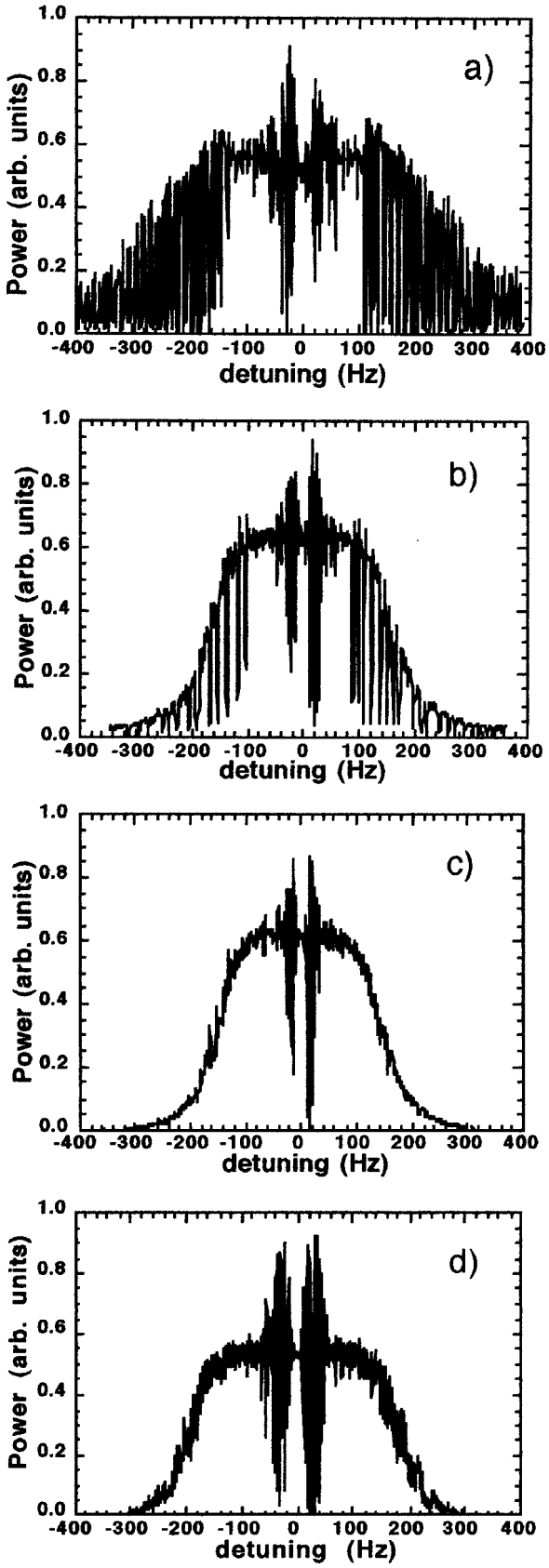

FIG. 12. Detuning curves of the laser (average laser power vs the detuning expressed in frequency differences with respect to the rf frequency for exact synchronism between the electron bunch and the laser pulse) for four values of the current: (a) 91 mA, (b) 85.4 mA, (c) 84 mA, and (d) 80 mA.

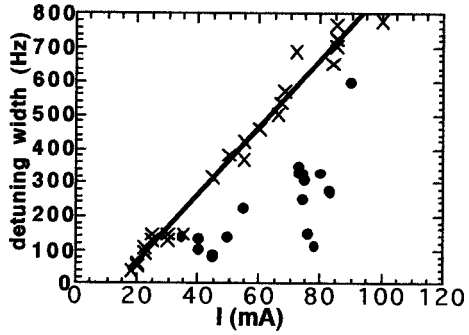

FIG. 13. Detuning curve width vs the total current in the ring (×), linearly growing with current except for the points below the line due to poor mirrors adjustment (●).

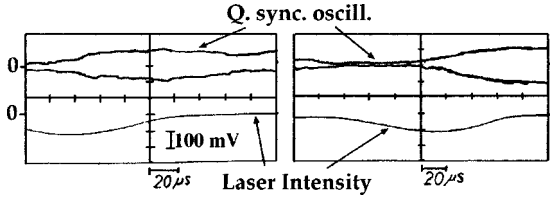

FIG. 14. Envelope of the quadrupolar coherent synchrotron oscillations (upper trace) measured with the dissector in the phase oscillation mode. Laser intensity is the lower trace.

on the detuning. Numerical simulations with an iterative model in the frequency domain [25] confirm the presence of the five areas shown in the experimental results.

Figure 12 shows measured detuning curves versus current. For the Super-ACO FEL operated with the quadrupolar feedback, seven areas are observed with two pulsed zones for larger detuning in addition to the usual five [Fig. 12(a)]. The detuning curve width becomes smaller when the current decreases. The two additional zones disappear below 85 mA [Fig. 12(b)] and the detuning curve recovers the usual five areas pattern [Fig. 12(c)]. The presence of seven zones could be attributed to the increase of the laser gain due to the damping of the quadrupolar coherent synchrotron oscillations. For example, a slightly higher gain on the UVSOR FEL with the installation of the new helical undulator led to the presence of two additional zones. Yet, the change from seven zones to five zones occurs precisely at 85 mA, which is also the threshold for the sextupolar coherent synchrotron oscillations. Thus, one could imagine that the two additional zones could be related to their presence. Clearly, the degradation of the beam stability resulting from the coherent modes of coherent synchrotron oscillation prevents ''cw'' operation of the FEL and introduces zones where the FEL is erratically pulsed adjacent to zones where the FEL adopts its natural macropulsed regime.

The width of the laser detuning curve is linearly dependant on the current (Fig. 13). However, the width can be reduced by poor transverse overlap due to a slow drift of the beam transverse dimensions or due to mechanical deformation of the mirror surface heated by the absorbed synchrotron radiation power (see the points before mirrors readjustments). The detuning curve also narrows due to the decrease of the electronic distribution width versus current. Therefore, it appears more advantageous to operate the FEL at high current with a larger detuning curve width. As a result in the central zone, the most interesting for users, the laser can be kept ''cw'' even with a slight detuning (over 10 Hz) and the jitter is easier to stabilize using the longitudinal feedback.

V. FEL STABILITY AND EFFECT OF THE LASER ON THE BEAM

The FEL operation strongly depends on the beam longitudinal stability. Without the quadrupolar feedback, the laser can be stabilized with the longitudinal feedback on the laser position, reducing significantly the laser jitter (20 ps), spectral drift (0.001 Å), and intensity fluctuations (1%) in the current range below the threshold for coherent quadrupolar modes. We will now consider the case of the laser operating in the 60–90-mA range, without the quadrupolar feedback. Once the laser starts, it totally suppresses quadrupolar modes but not the sextupolar modes starting above 85 mA. We observe a competition between the ring-induced collective oscillations and the heating effect of the laser. It seems that gain reduction due to the sextupole oscillations is not significant as compared with that of the quadrupole modes. The intensity begins to decrease just after the excitation of the quadrupole oscillation (see Fig. 14). Due to this competition, the intensity of the laser fluctuates, and the laser macrostructure becomes unstable and pulsed [8]. It is thus impossible to activate the longitudinal feedback. The collective oscillations change the longitudinal bunch profile and increase the beam energy spread, strongly decreasing the gain. Because of the collective motion of the bunch, the laser never reaches equilibrium. The resulting unstable macrostructure has a large linewidth, 1.2 Å, dispersed between 0.7 and 2.5 Å, while below 60 mA, with the longitudinal feedback, the line width is narrower and more stable, 0.4 Å on average dispersed between 0.3 Å and 0.76 Å. In addition, the collective oscillations of the bunch produce a significant wavelength drift, more than 12 Å over 3 min.

When the quadrupolar feedback is used, the sextupolar modes of coherent synchrotron oscillations are damped by the laser action (see Fig. 15). According to the saturation process model, the laser increases the energy spread in an incoherent way. At each interaction point of the laser wave, different electrons inside the bunch see a slightly different perturbation, so the bunch cannot evolve coherent and the coherent synchrotron oscillations are prevented [29]. Indeed, the laser acts as a feedback system to prevent coherent synchrotron oscillations.

Moreover, the laser has a ''cw'' zone at perfect tuning, where the longitudinal feedback can be used. Due to the QFB, the laser can be kept ''cw'' in this perfect tuning area and its jitter will be smaller [Fig. 16(c)]. In contrast the laser will be naturally more unstable in intensity and in position [Figs. 16(a) and 16(b)] without the QFB. Due to the longitudinal feedback on the laser position, the jitter is efficiently reduced [Fig. 16(d)] to 13 ps on average, with 4 and 30 ps at its extreme values. Therefore, with the QFB and the longitudinal laser feedback, the laser can be kept cw at the perfect tuning condition without any other adjustments of the electron beam from 100 mA down to 30 mA over 8 h of a user experiment.

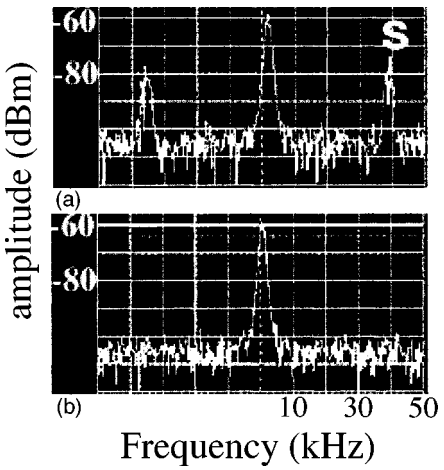

FIG. 15. Images from a Marconi spectrum analyzer, vertical axis: −10 dB m/div, horizontal axis: 10 kHz/div for a total current of 104 mA in the ring. In (a), sextupolar coherent synchrotron oscillations from each side of the bunch line at 38 kHz FEL off. In (b), FEL on, sextupolar coherent synchrotron oscillations are damped.

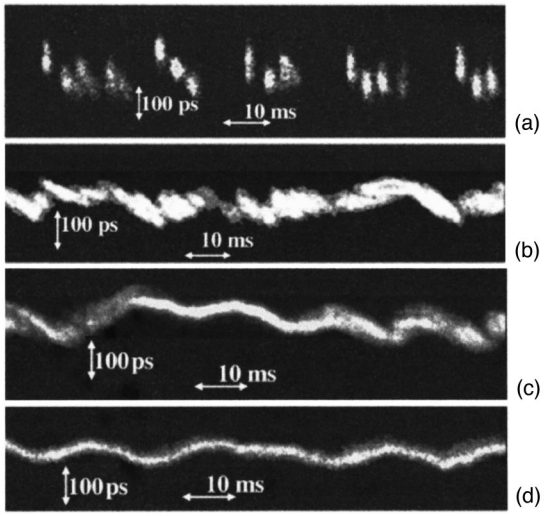

FIG. 16. Double sweep streak camera images of the FEL recorded over 100 ms for 3 configurations at high current. In (a) and (b), quadrupolar and longitudinal feedback are off at 87 mA, in (c) quadrupolar feedback is on and the longitudinal feedback is off at 90 mA, and in (d), both are on at 91.5 mA.

VI. CONCLUSION

Three feedback systems that damp the most important instabilities are necessary for a stable operation of the FEL: (i) dipolar feedback, (ii) quadrupolar feedback, and (iii) longitudinal feedback. Under these conditions, the Super-ACO FEL is able to operate at high current up to 120 mA and the useful average extracted power is increased and the stability improved. This has allowed us to perform user experiments that have provided both original and reliable data, thus confirming the interest of the SRFEL as a coherent UV light source for applications experiments. In addition, the operation of the FEL at higher current increases the compatibility with the synchrotron radiation users of Super-ACO. Moreover, the new temporal behavior, which has been observed, shows the complexity of the ''laser+electron beam'' system and the extreme sensitivity of the FEL to longitudinal beam instabilities. Nevertheless, to further improve the stabilization, the transverse evolution of the beam and of the laser should be carefully followed and possible instabilities damped. Therefore, for future SRFELs, very strict conditions on the beam stability are required, and feedback systems should be foreseen.

ACKNOWLEDGMENTS

We would like to thank T. Hara for his contribution to the work, A. Delboulbé and B. Visentin for their help during the FEL shifts, G. Flynn, J. Darpentigny, and L. Cassinari for the realization of the quadrupolar feedback, the Super-ACO operator group, and D. Jaroszinski and G. Flynn for their comments on the manuscript.

[1] D. A. G. Deacon, L. R. Elias, J. M. J. Madey, G. L. Ramian, H. A. Schwettman, and T. I. Smith, Phys. Rev. Lett. **38**, 892 (1977).

[2] T. Tomimasu, E. Oshita, S. Okuma, K. Wakita, T. Takii, S. Nishihara, A. Nagai, H. Tongu, K. Wakisaka, Y. Miyauchi, K. Saeki, and A. Kobayashi, Nucl. Instrum. Methods Phys. Res. A **393**, 188 (1997).

[3] P. G. O'Shea *et al.*, Nucl. Instrum. Methods Phys. Res. A **341**, 7 (1994).

[4] M. Billardon, P. Elleaume, J. M. Ortega, C. Bazin, M. Bergher, M. Velghe, Y. Petroff, D. A. G. Deacon, K. E. Robinson, and J. M. J. Madey, Phys. Rev. Lett. **51**, 1652 (1983).

[5] M. E. Couprie, P. Tauc, F. Merola, A. Delboulbé, T. Hara, and M. Billardon, Rev. Sci. Instrum. **65**, 1495 (1994).

[6] M. Marsi, M. E. Couprie, L. Nahon, D. Garzella, A. Delboulbé, T. Hara, R. Bakker, G. Indlekofer, M. Billardon, M. Billardon, and A. Taleb-Ibrahimi, Appl. Phys. Lett. **70**, 895 (1997).

[7] M. E. Couprie, V. Litvinienko, D. Garzella, A. Delboulbé, M. Velghe, and M. Billardon, Nucl. Instrum. Methods Phys. Res. A **331**, 37 (1993).

[8] M. E. Couprie, T. Hara, D. Gontier, P. Troussel, D. Garzella, A. Delboulbé, and M. Billardon, Phys. Rev. E **53**, 1871 (1996).

[9] M. E. Couprie, D. Garzella, J. H. Codarbox, and M. Billardon, Nucl. Instrum. Methods Phys. Res. A **358**, 374 (1995).

[10] E. I. Zinine, Nucl. Instrum. Methods Phys. Res. A **208**, 439 (1983).

[11] M. E. Couprie, V. M. Popik, E. I. Zinine, A. Delboulbé, D. Garzella, M. Velghe, and M. Billardon, Nucl. Instrum. Methods Phys. Res. A **318**, 59 (1992).

[12] F. J. Sacherer, IEEE Trans. Nucl. Sci. **20**, 825 (1973).

[13] M. E. Couprie, M. Velghe, D. Jaroszynski, and M. Billardon, Nucl. Instrum. Methods Phys. Res. A **304**, 58 (1991).

[14] P. B. Wilson, R. Servranckx, A. P. Sabersky, J. Gareyte, G. E. Fischer, A. W. Chao, and M. H. R. Donald, IEEE Trans. Nucl. Sci. **24** 3, 1211 (1977).

[15] J. M. Byrd and J. N. Corlett, *EPAC94 Conference Proceedings* (World Scientific, Singapore 1994), p. 1079.
[16] K. Wille and DELTA group, *EPAC96 Conference Proceedings* (Institute of Physics, Publishing, Bristol, 1996), pp. 95–99.
[17] F. Pedersen and F. J. Sacherer, IEEE Trans. Nucl. Sci. **24**, 1396 (1977).
[18] R. Roux, M. E. Couprie, T. Hara, R. J. Bakker, B. Visentin, and M. Billardon, Nucl. Instrum. Methods Phys. Res. A **393**, 33 (1997).
[19] H. Hama, J. Yamazaki, T. Kinoshita, K. Kimura, and G. Isoyama, Nucl. Instrum. Methods Phys. Res. A **358**, 365 (1995).
[20] A. H. Lumpkin, B. X. Yang, and Y. C. Chae, Nucl. Instrum. Methods Phys. Res. A **393**, 50 (1997).
[21] R. J. Bakker, M. E. Couprie, L. Nahon, D. Nutarelli, R. Roux, A. Delboulbé, D. Garzella, A. Nadji, B. Visentin, and M. Billardon, *EPAC96 Conference Proceedings* (Ref. [16]), p. 667.
[22] J. M. J. Madey, J. Appl. Phys. **42**, 1906 (1971).
[23] W. B. Colson, Nucl. Instrum. Methods Phys. Res. A **237**, 1 (1985).
[24] D. Garzella, M. E. Couprie, and M. Billardon, Nucl. Instrum. Methods Phys. Res. A **375**, 39 (1996).
[25] T. Hara, M. E. Couprie, and M. Billardon, Nucl. Instrum. Methods Phys. Res. A **375**, 67 (1996).
[26] T. Hara, M. E. Couprie, A. Delboulbé, D. Garzella, L. Nahon, and M. Billardon, Nucl. Instrum. Methods Phys. Res. A **358**, 341 (1995).
[27] H. Hama, K. Kimura, M. Hosaka, J. Yamazaki, and T. Kinoshita, Nucl. Instrum. Methods Phys. Res. A **393**, 23 (1997).
[28] M. Billardon, D. Garzella, and M. E. Couprie, Phys. Rev. Lett. **69**, 2368 (1992).
[29] G. Dattoli and A. Renieri, Nucl. Instrum. Methods Phys. Res. A **375**, 1 (1996).
[30] A. Renieri, Nuovo Cimento B **53**, 160 (1979).